Journal of Magnetic Resonance **146,** 290–296 (2000)
doi:10.1006/jmre.2000.2147, available online at http://www.idealibrary.com on IDEAL®

Magnetic Resonance Imaging of Coronary Arteries and Heart Valves in a Living Mouse: Techniques and Preliminary Results

Jan Ruff,* Frank Wiesmann,† Titus Lanz,* and Axel Haase*

**Physikalisches Institut, EP 5, and †Medizinische Klinik, Universität Würzburg, D-97074 Würzburg, Germany*

E-mail: haase@physik.uni-wuerzburg.de

Received February 8, 2000; revised June 14, 2000

New investigations in MRI of a mouse heart showed high-contrast cardiac images and thereby the possibility of doing functional cardiac studies of *in vivo* mice. But is MRI, in addition, capable of visualizing microstructures such as the coronary arteries and the heart valves of a living mouse? To answer this question, 2D and 3D gradient echo sequences with and without flow compensation were used to image the coronary arteries. To increase signal-to-noise ratio, a birdcage resonator was optimized for mouse heart imaging. Contrast between blood and myocardium was achieved through the inflow effect. A segmented three-dimensional FLASH sequence acquired with a multiple overlap thin slab technique showed the best results. With this technique an isotropic resolution of 100 μm was achieved. The left coronary artery could be visualized up to the apex of the heart. This is demonstrated with short axis views and 3D surface reconstructions of the mouse heart. The four cardiac valves were also visible with the 3D method.

Key Words: **mice; coronary angiography; cardiac valves; three-dimensional; magnetic resonance imaging.**

INTRODUCTION

Mouse models have become more and more popular in different fields of basic research. This is due to the current possibility of constructing mouse models with distinct genetic modifications such as gene overexpression, mutation, and knockout. Recently, it was shown that MRI is an excellent tool for investigating myocardial function and mass in adult (*1–5*) and even in newborn mice (*6*). Cardiac motion artifacts can be minimized with electrocardiographic (ECG)-triggered sequences. Focusing on short echo (TE) and repetition times (TR), segmented *k*-space FLASH (*f*ast *l*ow *a*ngle *sh*ot) sequences (*7, 8*) can perform high-quality mouse heart images (*5*) even at a typical murine heart rate (HR) of 500 to 630 beats per minute. The contrast between the big heart structures, such as the myocardium, and the heart chambers is sufficient to investigate cardiac function and myocardial mass.

Still up to now no method which could visualize cardiac microstructures including heart valves and coronary arteries of an *in vivo* mouse heart has been presented. Several human cardiac studies have shown the advantages and disadvantages of two-dimensional (2D) versus three-dimensional (3D) techniques (*9–14*). The main advantage of 2D sequences is the short acquisition time, so that one slice can be imaged within one breathhold. Three-dimensional imaging includes a higher signal-to-noise ratio (SNR) per acquisition time than of the multislice technique (*15*) and a higher possible resolution in the third dimension. However, due to the long acquisition time, most ECG-triggered 3D sequences cannot be implemented in combination with a single breathhold technique. Therefore most ECG-triggered 3D sequences of human coronary vessels suffer under a negative respiratory motion effect (*16*). It has been shown that respiratory navigation can reduce this breathing-dependent motion artifact (*17*); however any navigation technique prolongs the acquisition time. A new approach in human coronary angiography is VCAT (*v*olume *c*oronary *a*ngiography with *t*argeted scans) (*18*). The 3D slabs are positioned along the major axis of the coronary vessels. Each 3D slab can be acquired during a single breathhold; however it needs a lot of experience to find these positions in a suitable time.

For coronary angiography (CA) of the mouse, the key problems are similar to human CA. The fast beating of the mouse heart demands ultrafast imaging techniques to minimize motion artifacts. The small size of the mouse heart with its length of less than 10 mm requires high-resolution images to distinguish small cardiac structures. To visualize coronary vessels with a proximal diameter of 100–200 μm (*19*), high resolution must be realized not only in plane but in all three dimensions. Due to the assumed small voxel size, the radio frequency (RF) coil must be optimized with respect to the size of the mouse heart to achieve the highest possible sensitivity. The purpose of this study was to investigate the feasibility of magnetic resonance imaging to explore murine cardiac microstructures and coronary vessels.

Therefore, an optimized birdcage resonator was constructed to ensure the maximum possible SNR. Different gradient echo (GE) sequences were implemented and tested by varying contrast-specific NMR parameters (TR, flip angle, slice thickness).

1090-7807/00 $35.00

The results of three major sequences—a segmented 2D FLASH, a conventional 3D GE, and a segmented 3D FLASH sequence—acquired with a multiple thin slap technique (*15*), are described and the images of the best sequence are presented.

MATERIALS AND METHODS

Mouse preparation. Young mice (body weight 14–18 g) were anesthetized with 1.5 vol% Isoflurane. Electrocardiogram wires were attached to the front paws which were wrapped with thin copper foil. The ECG trigger signal was taken from a homebuilt ECG unit with adjustable trigger level and trigger delay (*20*). The heart rate of anesthetized mice ranged from 330 to 500 beats per minute. During the NMR experiment the mouse was positioned supine on a homebuilt warming pad to maintain constant body temperature throughout the MR study.

Hardware. We used a 7 T Bruker BIOSPEC 70/20 scanner (Bruker, Ettlingen, Germany). The system was equipped with a BIOSPEC G060 gradient system capable of 870 mT/m maximum gradient strength and 280 μs rise time. A laboratory-built eight-rung birdcage (*21*) was used for both spin excitation and signal detection. This birdcage was optimized for mouse heart imaging: The coil length of 20 mm at a coil diameter of 24 mm guaranteed a good sensitivity in the center of the probehead. Due to the shortness of the birdcage, the sensitivity drops about 10% within a range of 10 mm in the z direction. Thus, the filling factor of the coil was optimized for mouse hearts with a typical length of 10 mm or less. In order to increase the sensitivity by a factor of $\sqrt{2}$, the coil was quadrature driven (*22*).

MRI sequences. Regarding the ultrasmall size of the structures of interest, the following technical requirements must be fulfilled for all sequences:

The resolution must be below $(200\ \mu\text{m})^3$, because the diameter of the proximal coronary arteries is 100–200 μm (*19*), and the estimated thickness of the valve leaflets is about 100 μm.

The sequences must be ECG triggered and the k-space lines must be acquired during the diastole for two reasons: The heart's motion is minimal during this heart phase, so that data sampling during diastole prevents heart motion artifacts. The maximal blood volume flow within coronary arteries occurs during diastole and therefore the wanted inflow effect is maximized.

The upper heart rate of anesthetized mice at rest is about 500 bpm, corresponding to an RR interval of 120 ms. Assuming that the duration of the diastole is half a heart cycle, the sampling of k-space lines must take place within an acquisition window of 60 ms.

Three different types of heart-triggered sequences were implemented and optimized: A segmented 2D FLASH sequence (*7, 8*), a conventional 3D GE sequence (*23*), and a segmented 3D multiple thin slab FLASH sequence (*15*). All sequences were triggered by the R wave of the ECG signal. Data acquisition occurred at middle diastole. In order to minimize flow and motion-related image artifacts, two different concepts were applied:

- On one hand, the shortest possible echo time (TE) of 1.5 ms was utilized in 2D and 3D sequences. In addition, the 3D slabs were oriented perpendicular to the proximal left coronary arteries, in order to minimize in plane blood flow. This method is applicable to mouse CA, because typically the murine coronary artery system, which is different from human anatomy, lacks a left circumflex (*24*).
- On the other hand, flow compensation in the read direction was implemented, which extended TE to 2.4 ms.

The echo center was at the 64th point in a 256-point readout period. The TR of the segmented sequences was 4.6 ms. The flip angle was about 40°. A field-of-view of 25 $\times$ 25 mm was employed. With a matrix size of 256 $\times$ 256, the nominal in-plane resolution was 100 μm. To elevate SNR and to further reduce motion artifacts the complete images were averaged six times (serial averaging) (*25*). Fat suppression was not necessary, as the hearts of the mice studied with 14–18 g body weight did not show any epicardial fat. This was consistent with findings in autopsy. It was shown that respiratory navigation of MRI of a living mouse is feasible and bears the potential of significant image improvement, particularly of abdominal structures. However navigator-corrected images of the heart showed only minor improvement of edge definition and image contrast (*26*). Thus, respiratory triggering or gating was not implemented in this study.

The *segmented 2D FLASH sequence* was realized with short TE, as described above, and a section thickness of 500 μm. Eight segmented phase steps were acquired over 36.8 ms during consecutive diastolic heart phases. The complete k-space was acquired within 32 RR intervals in about 4 s.

For the *conventional 3D GE sequence* a section thickness of 6.4 mm was excited. The flip angle was 90°. The acquisition of one echo per heart cycle leads to TR equal to the time of one heart cycle (1/HR). Thirty-two phase steps in the second direction resulted in a resolution of 200 μm in the slab direction.

The section thickness of the *segmented 3D multiple thin slab FLASH sequence* was optimized with regard to achieving the largest possible slab thickness without loss of blood tissue contrast. Stepwise increasing the slab thickness from 1.6 to 6.4 mm, an excited thickness of 3.2 mm was found to be an ideal compromise. With 16 phase increments in the second phase direction, a resolution of 200 μm in the third dimension was achieved. The slab orientation was chosen as a transverse section or as a double-oblique short axis view. The short axis view has the advantage that the main left coronary arteries are oriented perpendicular to the slab. This increases inflow contrast and reduces flow artifacts (also from the ventricular blood). A sinc pulse with two loops was used as RF excitation

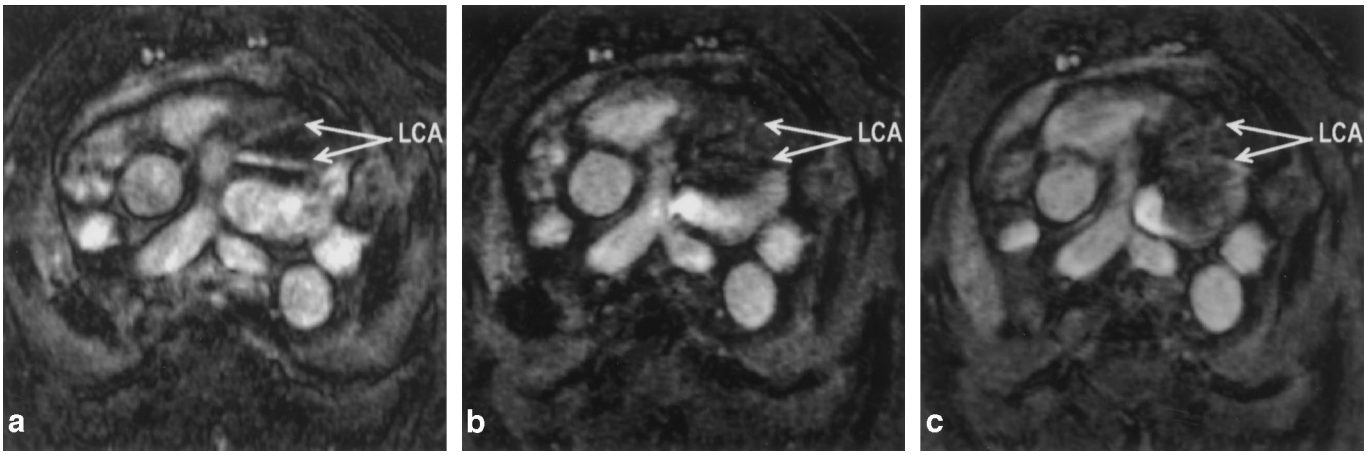

FIG. 1. Transverse slice acquired with the segmented 3D FLASH sequence. (a) The phase direction is chosen in the direction of the bifurcating LCA. The blood within the LCA is imaged with high signal intensity. (b) The read direction is set parallel to the proximal LCA. The coronary artery blood signal vanishes completely. (c) First-order flow compensation in the read direction cannot completely compensate for the dephasing effect of the read gradient.

pulse. We chose a slab overlap of 9/16 (*15*), so that 7 of the 16 acquired slices were used for the 3D data set. This overlap was necessary due to the low contrast in the slab periphery. To approach steady-state conditions and suppress tissue signal, 8 dummy pulses with a flip angle of approximately 30° were applied immediately prior to the imaging segment. The measurement time T_{slab} for each 3D slab was 6–9 min, depending on TR (which corresponds to the RR interval (RR)) and the number of averaged experiments (NEX = 6). This can be evaluated by

$$T_{slab} = RR \times N_{phase\ 2D}/N_{echoes} \times N_{phase\ 3D} \times NEX,$$

where $N_{phase\ 2D}$ and $N_{phase\ 3D}$ are the number of phase increments in the first and second phase direction, respectively. N_{echoes} is the number of acquired echoes per RR interval. The complete heart could be imaged with 7 to 8 slabs in approximately 1 h (without image processing). Within this time, the heart rate can vary, which leads to an acquisition of MR data in a slightly different heart phase. This problem was avoided by monitoring the ECG signal and phase gradient signal simultaneously on one oscilloscope. When the heart rate increased significantly, the trigger delay, which was realized as an hardware trimmer, was reduced manually to reset the end of the acquisition window to the beginning of the QRS complex.

Postprocessing. Postprocessing of the discrete data sets acquired with the multiple thin slab technique was necessary to achieve a composed high-contrast 3D data set. The raw data were filtered with a Gaussian high-pass filter to damp the signal of large structures, especially the myocardium (*27*). With this filter, the contrast between coronary arteries and myocardium could be significantly improved. Zerofilling of the raw data to 512 × 512 × 64 (double zerofill in plane and fourfold zerofill in the second phase direction) was applied to enhance the visualization of the small coronary arteries. Data were Fourier transformed and the overlapping slabs were merged to a single 3D data set. Short axis slices were chosen directly from this data set.

Three-dimensional visualization was done with AMIRA software (ZIP, Berlin, Germany). For a rapid illustration of the coronary course, the mouse heart must be cut out of the 3D data set to rid the view of the heart from pulmonary vessels. Then a surface visualization of distinct intensity values by a simple threshold algorithm is sufficient. For the surface visualization we used AMIRA's automatic threshold segmentation in three dimensions. The different compartments such as left ventricle (LV), right ventricle (RV), left coronary (LCA), and right coronary artery (RCA) were manually separated at their connections and allocated to different colors to enhance the anatomy of the mouse heart.

RESULTS

Respiratory motion artifacts (well known from human heart imaging (*28*)) were not visible within the images acquired with the sequences described.

The 2D technique with a section thickness of 500 μm was not able to depict any coronary artery in plane. Only a perpendicular cut through the coronary vessel could visualize its lumen as a highlighted point at the epicardial border of the myocardium.

With the conventional 3D GE sequence, only proximal coronary vessels could be depicted. The blood signal of these vessels waned within the first half of the slab. Best results were obtained with the segmented 3D FLASH sequence with a slab thickness of 3.2 mm.

In most examined mice, the proximal left coronary artery could be seen within a transverse slab positioned at the place of

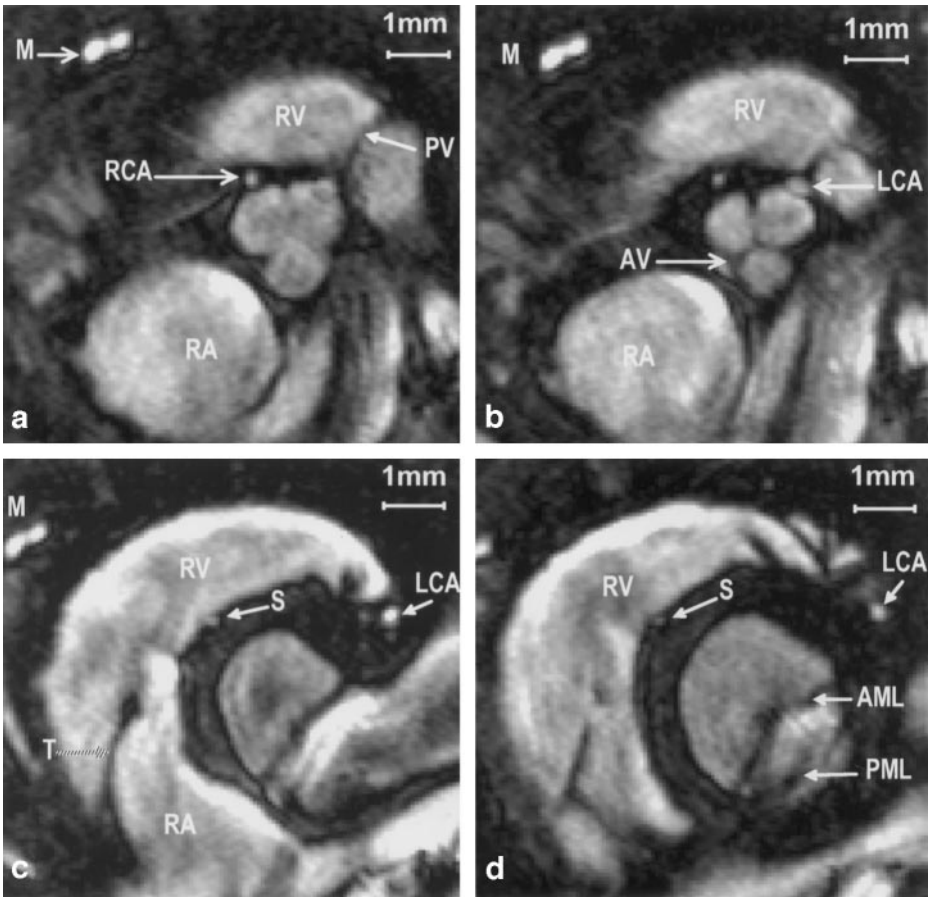

FIG. 2. Short axis view images acquired with the segmented 3D thin slab technique. RV, right ventricle; RA, right atrium; AR, aortic root; RCA, right coronary artery; LCA, left coronary artery; M, internal mammary artery and vein; S, septal coronary artery. (a) The RCA divides into two branches. The pulmonary valve (PV) separates RV and the pulmonary artery. (b) The LCA short after its origin and the three leaflets of the aortic valve (AV). (c) One leaflet of tricuspid valve (T) between RV and RA. The LCA passes between RV and the left atrium. S is visible at the border of septum and RV. (d) AML, anterior mitral leaflet, PML, posterior mitral leaflet, and the proximal LCA. S is still identifiable.

the aortic root. However, sometimes the blood of the coronary vessel, which proceeds a few millimeters in plane, was imaged as black blood (Fig. 1b), caused by spin dephasing. Switching the phase gradient parallel to the blood flow direction minimized this dephasing effect, as demonstrated in Fig. 1a. However blood flow in the coronary vessels is not unidirectional, and it is not possible to align the phase gradient in the direction of all vessels. Gradient moment nulling (*29*) should reduce the flow dephasing effects, but the implemented first-order flow compensation in the read direction could not completely prevent the flow-dependent dephasing effect, as shown in Fig. 1c. To avoid dephasing effects and benefit simultaneously from shortest possible TE, the 3D slabs were oriented as short axis slabs and no flow compensation gradients were further used. With this technique we gained high-contrast cardiac images:

Large structures, such as the LV and RV, the left and right atrium, and the aortic root, could be imaged with great detail (Figs. 2a–2c). The four cardiac valves (pulmonary valve (Fig. 2a), aortic valve (Fig. 2b), tricuspid valve (Fig. 2c), and mitral valve (Fig. 2d)) were clearly visible in the acquired diastolic heart phase. Within the short axis views of Fig. 2, the LCA and RCA were well identifiable: Figure 2a shows the proximal RCA and its division. In Fig. 2b the LCA is imaged short after its origin. The LCA is further visible in Figs. 2c and 2d as indicated. In addition, a septal coronary artery (S) was identified. This vessel has its origin in the RCA and courses at the border of the septum and the RV (Figs. 2c and 2d).

Any oblique slice can be reconstructed from the 3D data set. The coronal oblique slice in Fig. 3a shows large structures such as the LV, RV, and the aortic root, as well as microstructures such as the proximal LCA and the pulmonary and aortic valves. The stripes within this picture are caused by the discrete slab acquisition. The signal intensity variation at the slab borders depends on inflow and outflow effects of ventricular blood. Nevertheless, the border line of LV and RV courses continuously and the LCA is depicted without discontinuities. Figure 3b shows the longest possible representation of the LCA within one plane. It illustrates the difficulty to find such a plane with 2D techniques during the MR experiment. The particular oblique orientation also varies from object to object.

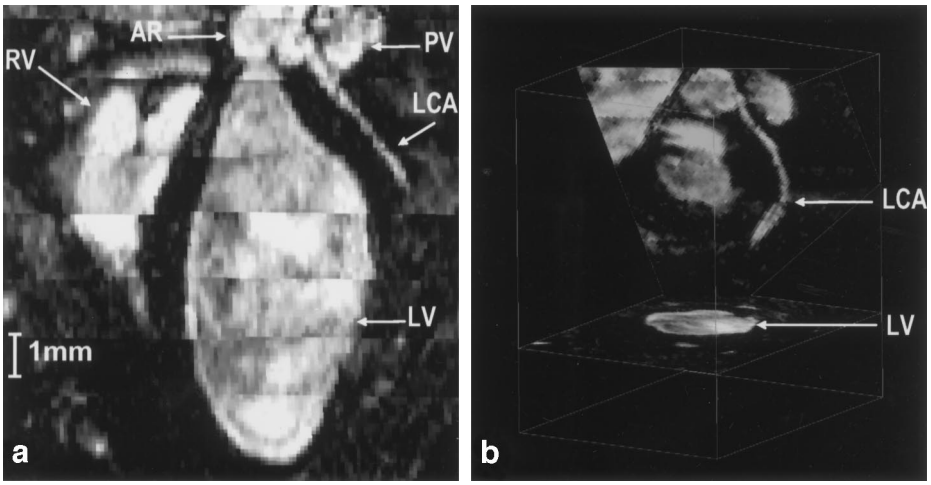

FIG. 3. (a) Coronal oblique slice reconstruction with RV, LV, AR, PV, and proximal LCA. (b) Reconstruction of an oblique slice with maximum length of the LCA. The lower image shows a midventricular short axis view with LV, apex of RV, and a branch of the LCA.

Due to the tortuous course of the coronary arteries, the entire LCA cannot be depicted within one plane. Hereby, 3D surface visualization can help to show the complete course of detected coronary arteries. Figure 4 illustrates surface renderings of the segmented data set. Figure 4a represents the murine heart from the top. One can view inside the aortic root (dark red). The two RCA branches (yellow) run over the RV (blue). The LCA (yellow) is visualized from its origin to the apex of the heart. A lateral view (Fig. 4b) of the segmented compartments LV (red), left atrium (red), aortic root (dark red), RV, and LCA illustrates the ellipsoidal shape of the LV and the exact course of the LCA.

DISCUSSION

In human cardiac studies, respiratory motion causes ghosting and blurring artifacts (*28*). However mouse heart images acquired with GE sequences did not show any respiratory

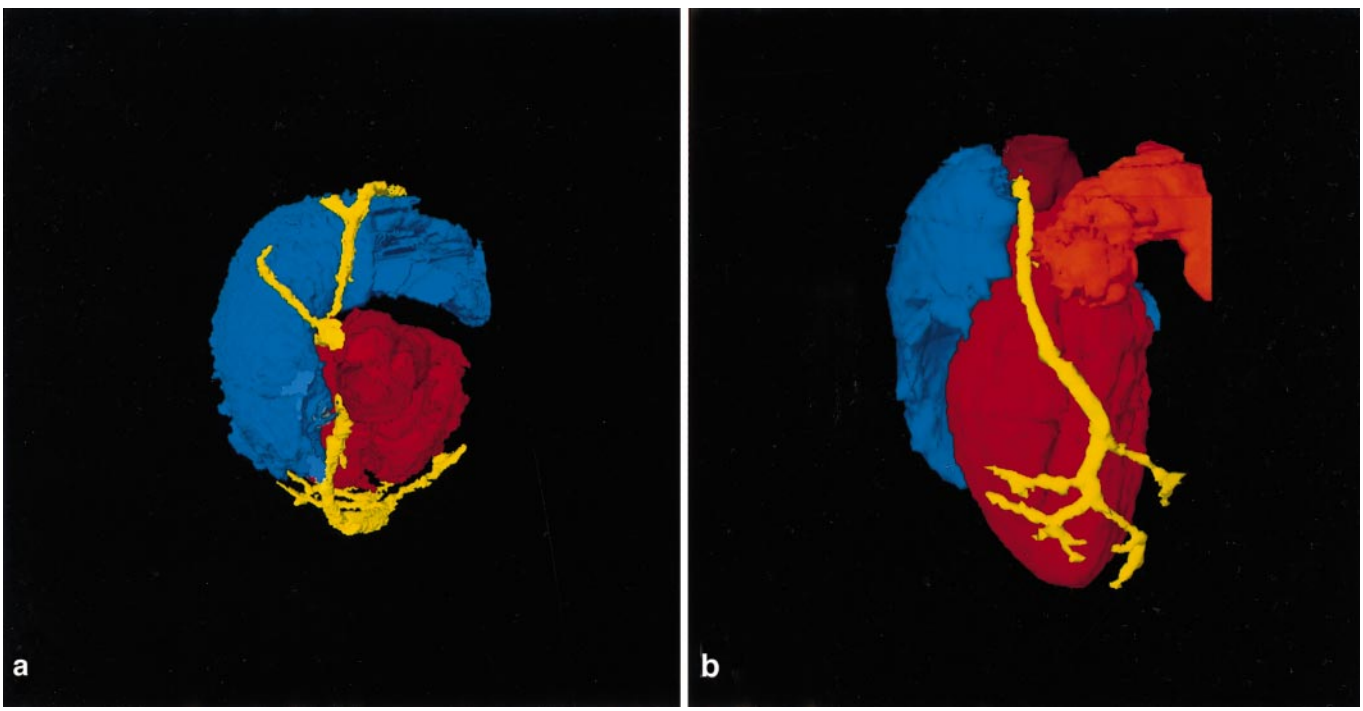

FIG. 4. Surface visualization of the segmented 3D data set. (a) View from the top with RV (blue), LV (red), aortic root (dark red), and coronary arteries (yellow). (b) Lateral view of LV (red), RV (blue), aortic root (dark red), left atrium (red), and left coronary vessel tree (yellow).

ghosting (*26*). Respiratory image disturbance could be inconspicuous in mouse heart imaging due to the low ratio of breathing rate to heart rate for anesthetized mice of 1:8 (*30*) (typical ratio for man is 1:4). The inspiration phase of anesthetized mice is, in addition, very short with respect to the total breathing cycle. This means that at maximum every 8th *k*-space line is missregistrated during the acquisition of the mouse heart. Multiple serial averaging (*25*) has further reduced respiratory ghosting and pulsating flow artifacts in cardiac mouse imaging, so that there was no need for respiratory-triggered or -navigated sequences.

The contrast between myocardium and coronary vessels is achieved with inflow effect of the blood. For 3D acquisition, this inflow effect depends on T_1 of tissue in contrast to the effective T_1 of blood, which is related to the ratio of flow velocity to slab thickness of the stimulated spins.

The 3D GE sequence with a slab thickness of 6.4 mm has shown emphasized blood of a coronary vessel at the upper part of the excited section, but not at the end of the same vessel within this section. We assume that only the upper part of the slab is supplied with unsaturated spins during two excitation pulses due to the inflow of blood, whereas the blood in the distal vessels is replaced with the presaturated blood of the same section and therefore shows no contrast to the surrounding tissue. The blood flow velocity can be estimated by the division of the length of the enhanced vessel (L_{vessel}) and the RR interval:

$$v \approx \frac{L_{\text{vessel}}}{\text{RR}} \leq \frac{4 \text{ mm}}{120 \text{ ms}} = 3 \text{ cm/s}.$$

The 3D GE technique was effectually used in CA of the perfused rat heart, as was demonstrated by Roder and coworkers (*23*). The reasons for the feasibility of conventional 3D GE CA in the perfused heart model are the longer RR interval (200–250 ms) and the higher blood flow velocity in these coronary vessels.

With TR equal to one or two *in vivo* mouse RR intervals, it is not possible to image the complete coronary vessel tree with sufficient inflow contrast within one single acquisition due to high vessel blood saturation in the lower part of the excited 3D section.

Thus it was comprehensible that we obtained the best vessel tissue contrast for the *in vivo* mouse heart with the segmented 3D multiple thin slab technique (*15*). A slab thickness of 3.2 mm was just thin enough to take advantage of the inflow effect for the complete section. As we wanted to depict both coronary vessels and microstructures of the heart we sampled the data sets with this slab thickness. For microimaging of heart valves only, thicker slabs can be applied due to the higher flow velocities in the heart cavities.

Since the diameter of the coronary vessels is smaller than 200 μm (*19*), partial volume effect and blurring lead to an overestimated representation of the vessel in the radial direction. For the direct investigation of vasoactive drugs such as adenosine or endothelin 1, a resolution of 50 μm in plane and 100 μm in vessel direction should be realized. This nominal resolution can be acquired with TE = 1.5 ms similar to that of our approach. However, doubling the resolution in three dimensions requires a 64 times longer acquisition time to reach the same SNR. Thus, the measurement time per slab would increase to 6 h, which is too long for *in vivo* studies. Such studies should be performed with intravascular contrast agents.

CONCLUSION

With MRI, murine cardiac microstructures and major coronary vessels can be visualized. An RF resonator with optimized filling factor is crucial to detect the low signal of coronary vessel blood and to save acquisition time. Two-dimensional techniques have shown that the inflow effect is not sufficient to depict coronary arteries or veins in plane. The conventional 3D GE sequence has shown that the inflow of blood during one RR interval can only enhance the upper part of the coronary vessel tree.

Consequently, the segmented 3D multiple thin slab FLASH sequence achieved the best results. With this technique, the course of the left coronary arteries was depicted either as bifurcating into two major vessels as shown in Fig. 1 or as a single major LCA (Fig. 4). This result is in accordance with the findings of Michael *et al.* (*24*), who described these different coronary patterns of mice. The nominal resolution of 100 $\times$ 100 $\times$ 200 μm^3 was enough to visualize the major left and right coronary arteries, as well as all the four cardiac valves.

The multiple thin slab technique can further be used for MR angiography of any mouse vessel. An interesting application is the aortic banding model: The artificial aortic stenosis can now be verified and quantified *in vivo* and can be set in relation to the hypertrophic effect.

Recently apolipoprotein E-deficient mice (*31*) have been shown to develop lesions of atherosclerosis with characteristic distribution to those in humans. Sites of predilecions are the aortic root and the lesser curvature of the aortic arch (*32*). These mice could be investigated with the present technique to quantify the developmental changes of atherosclerotic plaques and their effects on ventricular function.

ACKNOWLEDGMENTS

The authors thank Ralf Deichmann for helpful discussion and Karlheinz Rein for his support in using AMIRA surface visualization tools. The figures in this paper have been created using the AMIRA visualization system developed at ZIB (http://amira.zib.de/). This work was supported by SFB 355 (Pathophysiologie der Herzinsuffizienz, Teilprojekte A1 und A6) and Graduiertenkolleg NMR (HA 1232/8-1).

REFERENCES

1. D. Burstein, MR imaging of coronary artery flow in isolated and in vivo hearts, *J. Magn. Reson. Imaging* **1,** 337–346 (1991).
2. S. E. Rose, S. J. Wilson, F. O. Zelaya, S. Crozier, and D. M. Doddrell, High resolution high field rodent cardiac imaging with flow enhancement suppression, *Magn. Reson. Imaging* **12,** 1183–1190 (1994).
3. T. Kubota, C. F. McTiernan, C. S. Frye, S. E. Slawson, B. H. Lemster, A. P. Koretsky, A. J. Demetris, and A. M. Feldman, Dilated cardiomyopathy in transgenic mice with cardiac-specific overexpression of tumor necrosis factor-alpha, *Circ. Res.* **81,** 627–635 (1997).
4. S. E. Slawson, B. B. Roman, D. S. Williams, and A. P. Koretsky, Cardiac MRI of the normal and hypertrophied mouse heart, *Magn. Reson. Med.* **39,** 980–987 (1998).
5. J. Ruff, F. Wiesmann, K-H. Hiller, S. Voll, M. von Kienlin, W. R. Bauer, E. Rommel, S. Neubauer, and A. Haase, Magnetic resonance microimaging for noninvasive quantification of myocardial function and mass in the mouse, *Magn. Reson. Med.* **40,** 43–48 (1998).
6. F. Wiesmann, J. Ruff, K-H. Hiller, E. Rommel, A. Haase, and S. Neubauer, Developmental changes of cardiac function and mass in neonatal, juvenile and adult mice analyzed with high resolution magnetic resonance imaging, *Am. J. Physiol.* **278,** H652–H657 (2000).
7. A. Haase, J. Frahm, M. Matthaei, W. Hänicke, and K. D. Merboldt, FLASH imaging, rapid NMR imaging using low flip angle pulses, *J. Magn. Reson.* **67,** 258–266 (1986).
8. D. J. Atkinson and R. R. Edelman, Cineangiography of the heart in a single breath hold with a segmented turbo FLASH sequence, *Radiology* **178,** 357–360 (1991).
9. C. L. Dumoulin, S. P. Souza, R. D. Darrow, and W. J. Adams, A method of coronary MR angiography, *J. Comput. Assist. Tomogr.* **15,** 705–710 (1991).
10. R. R. Edelman, W. J. Manning, D. Burstein, and S. Paulin, Coronary arteries: Breath-hold MR angiography, *Radiology* **181,** 641–643 (1991).
11. A. J. Duerinckx, MRI of coronary arteries, *Int. J. Card. Imaging* **13,** 191–197 (1997).
12. D. Li, C. B. Paschal, E. M. Haacke, and L. P. Adler, Coronary arteries, three-dimensional MR imaging with fat saturation and magnetization transfer contrast, *Radiology* **187,** 401–406 (1993).
13. M. B. Hofman, C. B. Paschal, D. Li, E. M. Haacke, A. C. van Rossum, and M. Sprenger, MRI of coronary arteries: 2D breath-hold vs 3D respiratory-gated acquisition, *J. Comput. Assist. Tomogr.* **19,** 56–62 (1995).
14. C. B. Paschal, E. M. Haacke, L. P. Adler, and D. Finelli, Magnetic resonance coronary artery imaging, *Cardiovasc. Intervent. Radiol.* **15,** 23–31 (1992).
15. D. L. Parker, C. Yuan, and D. D. Blatter, MR angiography by multiple thin slab 3D acquisition, *Magn. Reson. Med.* **17,** 434–451 (1991).
16. Y. Wang, T. M. Grist, F. R. Korosec, P. S. Christy, M. T. Alley, J. A. Polzin, and C. A. Mistretta, Respiratory blur in 3D coronary MR imaging, *Magn. Reson. Med.* **33,** 541–548 (1995).
17. Y. Wang, P. J. Rossman, R. C. Grimm, S. J. Riederer, and R. L. Ehman, Navigator-echo-based real-time respiratory gating and triggering for reduction of respiration effects in three-dimensional coronary MR angiography, *Radiology* **198,** 55–50 (1986).
18. P. A. Wielopolski, R. J. van Geuns, P. J. de Feyter, and M. Oudkerk, Breath-hold coronary MR angiography with volume targeted imaging, *Radiology* **209,** 209–219 (1998).
19. J. Thüroff, W. Hort, and H. Lichi, Diameter of coronary arteries in 36 species of mammalian form mouse to giraffe, *Basic Cardiol.* **79,** 199–206 (1984).
20. E. Rommel and A. Haase, An ECG trigger unit optimized for fast rat heart imaging, Abstracts of the Society for Magnetic Resonance, p. 938 (1995).
21. C. E. Hayes, W. A. Edelstein, J. F. Schenck, O. M. Mueller, and M. Eash, An efficient, highly homogeneous radiofrequency coil for whole-body NMR imaging at 1.5 T, *J. Magn. Reson.* **63,** 622–628 (1985).
22. C. N. Chen, D. I. Hoult, and V. J. Sank, Quadrature detection coils—A further $\sqrt{2}$ improvement in sensitivity, *J. Magn. Reson.* **54,** 324–327 (1983).
23. F. Roder, K-H. Hiller, P. Henz, M. von Kienlin, W. R. Bauer, G. Ertl, and A. Haase, Three-dimensional coronary angiography of the perfused rat heart, *J. Magn. Reson. Imaging* **7,** 316–320 (1997).
24. L. H. Michael, M. L. Entman, C. J. Hartley, K. A. Youker, J. Zhu, S. R. Hall, H. K. Hawkins, K. Berens, and C. M. Ballantyne, Myocardial ischemia and reperfusion, a murine model, *Am. J. Physiol.* **269,** H2147–H2154 (1995).
25. W. T. Dixon, M. E. Brummer, and J. A. Malko, Acquisition order and motional artifact reduction in spin warp images, *Magn. Reson. Med.* **6,** 74–83 (1988).
26. J. Ruff, F. Wiesmann, and A. Haase, High speed respiratory navigation applied to MR imaging of the living mouse, Abstracts of the International Society for Magnetic Resonance in Medicine, p. 1698 (2000).
27. R. Deichmann, F. Wiesmann, C. Hillenbrand, D. Hahn, and A. Haase, Contrast enhancement and artifact reduction in magnetization-prepared MR angiography, *Int. J. Imaging Syst. Technol.* **10,** 266–272 (1999).
28. C. L. Schultz, R. J. Alfidi, A. D. Nelson, S. Y. Kopiwoda, and M. E. Clampitt, The effect of motion on two-dimensional Fourier transformation magnetic resonance images, *Radiology* **152,** 117–121 (1984).
29. E. M. Haacke and G. W. Lenz, Improving MR image quality in the presence of motion by using rephasing gradients, *Am. J. Radiol.* **148,** 1251–1258 (1997).
30. J. Ruff, F. Wiesmann, K-H. Hiller, S. Neubauer, E. Rommel, and A. Haase, Influence of isoflurane anesthesia on contractility of mouse heart in vivo. A NMR imaging study, Abstracts of the European Society for Magnetic Resonance in Medicine and Biology, p. 169 (1998).
31. S. H. Zhang, R. L. Reddick, J. A. Piedrahita, and N. Maeda, Spontaneous hypercholesterolemia and arterial lesions in mice lacking apolipoprotein E, *Science* **258,** 468–471 (1992).
32. Y. Nakashima, A. S. Plump, E. W. Rains, J. L. Breslow, and R. Ross, ApoE-deficient mice develop lesions of all phases of atherosclerosis throughout the arterial tree, *Arteriosclerosis Thrombosis* **14,** 133–140 (1994).